Hindawi
Complexity
Volume 2022, Article ID 8080048, 11 pages
https://doi.org/10.1155/2022/8080048

WILEY | Hindawi

Research Article

Synchronous Reluctance Motor: Dynamical Analysis, Chaos Suppression, and Electronic Implementation

Balamurali Ramakrishnan,[1] **Andre Chéagé Chamgoué**,[2] **Hayder Natiq**,[3] **Jules Metsebo**,[4] **and Alex Stephane Kemnang Tsafack**[5]

[1]*Center for Nonlinear Systems, Chennai Institute of Technology, Chennai-600069, Tamilnadu, India*
[2]*Department of Basic Sciences, School of Geology and Mining Engineering, University of Ngaoundere, P. O. BOX 115, Meiganga, Cameroon*
[3]*Information Technology College, Imam Ja'afar Al-Sadiq University, Baghdad 10001, Iraq*
[4]*Department of Hydraulics and Water Management, National Advanced School of Engineering, University of Maroua, P. O. Box 46, Maroua, Cameroon*
[5]*Research Unit of Condensed Matter of Electronics and Signal Processing Department of Physics, Faculty of Sciences, University of Dschang, P. O. Box 67, Dschang, Cameroon*

Correspondence should be addressed to Jules Metsebo; jmetsebo@gmail.com

Received 7 September 2021; Revised 13 February 2022; Accepted 18 February 2022; Published 17 March 2022

Academic Editor: Jesus M. Munoz-Pacheco

Dynamical analysis, chaos suppression and electronic implementation of the synchronous reluctance motor (SynRM) without external inputs are investigated in this paper. The different dynamical behaviors (including monostable periodic behaviors, bistable periodic behaviors, monostable chaotic behaviors, and bistable chaotic behaviors) found in the SynRM without external inputs are illustrated in the two parameters largest Lyapunov exponent (LLE) diagrams, one parameter bifurcation diagram, and phase portraits. The three single controllers are designed to suppress the chaotic behaviors found in SynRM without external inputs. The three proposed single controllers are simple and easy to implement. Numerical simulation results show that the three proposed single controllers are effective. Finally, the dynamical behaviors found in the SynRM without external inputs and the physical feasibility of the three proposed single controllers are validated through circuit implementation on OrCAD-PSpice software.

1. Introduction

An electrical motor converts electrical energy into mechanical energy thank to the discovery by Michael Faraday in the 19th century. He stated that a current carrying coil within a magnetic field will experience a force. Electrical motors can be found in steel rolling mills, drilling machines, railway traction, industrial robots, and in most household items and office equipment [1–6]. Today, there are several variants of electric motors including the induction motor [7,8], permanent-magnet brushless motor [9–12], and variable-reluctance motor. The variable-reluctance motor class takes the advantages of a simple and rugged structure, good compatibility with the power converter, and high recyclability for the core and winding [13]. The variable-reluctance motor is divided into the switched reluctance motor [14,15] and synchronous reluctance motor (SynRM). The SynRM uses a distributed winding and sinusoidal wave which can essentially eliminate the torque pulsation and acoustic noise problems. It is broadly used in the field of transportation, industrial and agricultural production, commercial and household appliances, medical appliances and equipment, and so on [16–20]. Because of its advantage over other types of electrical motors in simple mechanical construction, there were no slip ring and no permanent magnet and over other

servomotors in high efficiency, high power density, and low manufacturing cost [21].

For industrial automation manufacturing, the secure and stable operation of the SynRM is an essential requirement because chaotic behaviors can extremely destabilize the SynRM and even cause the drive system to fail [20]. Hopf Bifurcation and chaos have been found in the SynRM [13]. In this paper, it is demonstrated that the SynRM can exhibit monostable periodic behaviors, bistable periodic behaviors, monostable chaotic behaviors, and bistable chaotic behaviors. The chaotic behaviors found in the SynRM induces instability in this motor and shortens its service time [9]. Thereafter, a variety of methods to control chaos have been used to suppress the chaotic behavior in SynRM. A passive adaptive controller [21], a nonlinear feedback controller [22], a controller based on tridiagonal structure matrix stability theory [23], a vector controller [24–26], a sliding mode controller [27], and an adaptive sliding mode controller [28] were used for the control of chaotic behavior in SynRM. Most of the existing techniques for the control of chaotic behavior in SynRM use a nonlinear and complicated controller.

To the best of authors' knowledge, no study on the chaos suppression in SynRM without external inputs has been carried out with the single state feedback controller. The single state feedback control method is simple, concise, and easy to implement. Therefore, the main contribution of this paper is to investigate the dynamical analysis of SynRM without external inputs and to design three single and simple controllers to suppress chaos in SynRM. The dynamical analysis and chaos suppression via a single controller of SynRM without external inputs are analytically, numerically, and electronically analysed in this paper. The dynamical analysis of SynRM without external inputs is investigated in Section 2. In Section 3, three proposed single controllers are employed to achieve the suppression of chaos in SynRM without external inputs. Section 4 presents the electronic implementation in order to check the existence of dynamical behaviors found in SynRM and the effectiveness of the three proposed single controllers. Finally, conclusions are given in Section 5.

2. Dynamical Analysis of SynRM without External Inputs

The SynRM can be described by the following rate equations [1, 2, 13]:

$$\frac{\mathrm{d}\widetilde{i}_d}{\mathrm{d}\widetilde{t}} = \frac{\left(\widetilde{u}_d - R_s\widetilde{i}_d + \omega_e L_q \widetilde{i}_q\right)}{L_d}, \tag{1a}$$

$$\frac{\mathrm{d}\widetilde{i}_q}{\mathrm{d}\widetilde{t}} = \frac{\left[-R_s\widetilde{i}_q - \omega_e L_d \widetilde{i}_d + k_p\left(\widetilde{\omega} - \omega_{\mathrm{ref}}\right)\right]}{L_q}, \tag{1b}$$

$$\frac{\mathrm{d}\widetilde{\omega}}{\mathrm{d}\widetilde{t}} = \frac{\left[3P\left(L_d - L_q\right)\widetilde{i}_d\widetilde{i}_q/4 - B\widetilde{\omega} + \widetilde{T}_L\right]}{J}, \tag{1c}$$

where $\widetilde{i}_d, \widetilde{i}_q$ are the d (direct)- and q (quadrature)-axis stator currents, $\widetilde{\omega}$ is the mechanical rotor speed, ω_e is the electrical rotor speed, $\widetilde{u}_d$ is the stator voltage on d axis, R_s is the stator resistance per phase, k_p is the feedback coefficient, and ω_{ref} is the reference rotor speed, L_d, L_q are the d- and q-axis stator inductors, P is the number of poles, J, $\widetilde{T}_L$, and B are the inertia constant of the motor and load, load torque, and viscous friction coefficient, respectively. The normalization of equations (1a)–(1c) leads to the following dimensionless form of the mathematical model of SynRM:

$$\frac{\mathrm{d}x}{\mathrm{d}t} = u_d - bx + yz, \tag{2a}$$

$$\frac{\mathrm{d}y}{\mathrm{d}t} = -y - xz + c\left(z - z_{\mathrm{ref}}\right), \tag{2b}$$

$$\frac{\mathrm{d}z}{\mathrm{d}t} = xy - az + T_L, \tag{2c}$$

with the following rescaling variables and parameters: $\tau = L_q/R_s, \widetilde{t} = \tau t, a = BL_q/(JR_s), \quad b = L_q/L_d, k = \sqrt{8J/[3bP^2(L_d - L_q)(L_q/R_s)^2]}, \quad \omega_{\mathrm{ref}} = \tau z_{\mathrm{ref}}, \quad x = [1/(bk)]\widetilde{i}_d, y = (1/k\widetilde{i}_q), z = (L_q/R_s)\widetilde{\omega}, c = 2k_d/(kPL_q), u_d = \widetilde{u}_d/(kR_s), T_L = P\tau^2\widetilde{T}_L/(2J)$. The external inputs are removed ($u_d = z_{\mathrm{ref}} = T_L = 0$), and System (2a)–(2c) becomes

$$\frac{\mathrm{d}x}{\mathrm{d}t} = -bx + yz, \tag{3a}$$

$$\frac{\mathrm{d}y}{\mathrm{d}t} = -y - xz + cz, \tag{3b}$$

$$\frac{\mathrm{d}z}{\mathrm{d}t} = xy - az. \tag{3c}$$

System (3a)–(3c) is invariant under the transformation: $(x, y, z) \Leftrightarrow (x, -y, -z)$ and dissipative if $\nabla V = (\partial(\mathrm{d}x/\mathrm{d}t)/\partial x) + (\partial(\mathrm{d}y/\mathrm{d}t)/\partial y) + (\partial(\mathrm{d}z/\mathrm{d}t)/\partial z) = -(a + b + 1) < 0$. It has only one equilibrium point $O(0, 0, 0)$ if $\Delta = c^2 - 4a < 0$, three equilibrium points $O(0, 0, 0)$, $E_{1,2}(c/2, \pm\sqrt{ab}, \pm c\sqrt{b/a}/2)$ if $\Delta = 0$, and five equilibrium points $O(0, 0, 0)$, $E_{11,21}((c + \sqrt{\Delta})/2, \pm\sqrt{ab}, \pm(c + \sqrt{\Delta})\sqrt{b/a}/2)$, $E_{11,21}((c - \sqrt{\Delta})/2, \pm\sqrt{ab}, \pm(c - \sqrt{\Delta})\sqrt{b/a}/2)$ if $\Delta > 0$ [13]. The linear stability analysis of system (2) revealed that the equilibrium points displayed Hopf bifurcation [13]. When the parameters a, b, c are varied, SynRM without external inputs can be expected to exhibit steady state, periodic, and chaotic behaviors. In order to identify the dynamical behaviors of SynRM without external inputs, two parameters LLE diagrams are constructed in Figure 1.

From Figure 1, periodic or steady state regions are characterized as a combination of light blue-light blue-green colors, and chaotic regions are characterized by yellow and red colors. For $b = 0.2$ and $c = 22$, the bifurcation diagrams and LLE of SynRM without external inputs as a function of the parameter a are plotted in Figure 2.

Figure 2 shows that the SynRM without external inputs exhibits monostable period-3 oscillations, bistable period-3

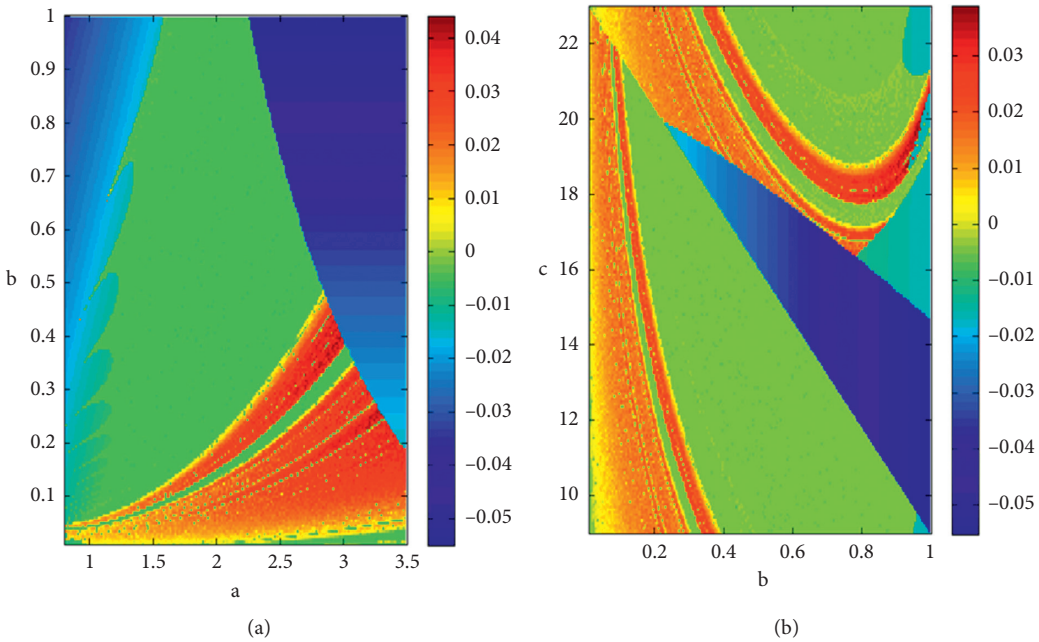

Figure 1: Two parameters LLE diagrams in (a) (a, b) space for $c = 22$ and (b) (b, c) space for $a = 1.53$.

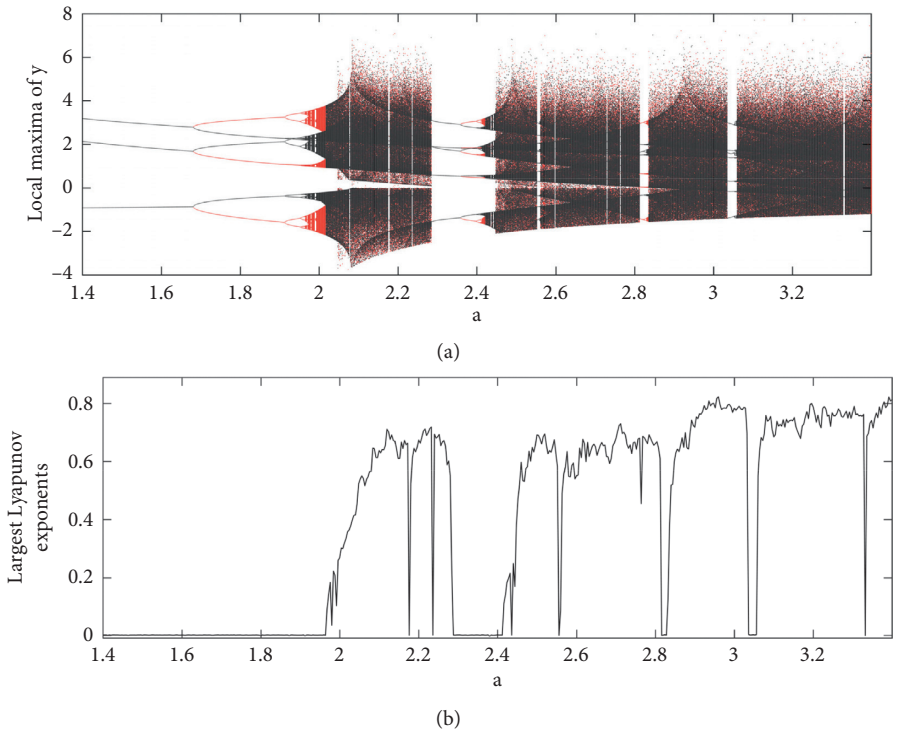

Figure 2: Bifurcation diagrams of $y(t)$ (a) and LLE (b) of SynRM versus the parameter a for $b = 0.2$ and $c = 22$. Bifurcation diagrams are obtained by scanning the parameter a upwards (black) and downwards (red). The initial conditions are $(x(0), y(0), z(0)) = (0.1, 0.2, 0.2)$.

oscillations followed to period tripling to bistable chaos and monostable chaos interspersed with bistable and monostable periodic regions. The dynamical behaviors shown in Figure 2 are illustrated in Figure 3 for a specific value of a.

The SynRM without external inputs exhibits monostable periodic attractors in Figure 3(a), bistable periodic attractors in Figure 3(b), bistable one-scroll chaotic attractors in Figure 3(c), and monostable double-scroll chaotic attractors in Figure 3(d). The bifurcation diagrams of SynRM without external inputs obtained numerically by the parameters b and c reveal monostable chaos and bistable chaos interspersed with monostable and bistable periodic regions

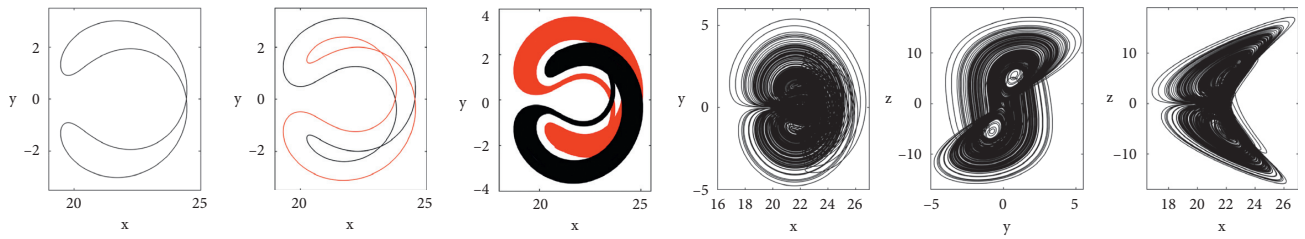

FIGURE 3: Phase planes of SynRM without external inputs for a specific value of parameter a: (a) $a = 1.5$, (b) $a = 1.8$, (c) $a = 2$, and (d) $a = 3$. The curves in black line are obtained by using the initial conditions $(x(0), y(0), z(0)) = (0.1, 0.2, 0.2)$, while the curves in red line are obtained by using the initial conditions $(x(0), y(0), z(0)) = (0.1, -0.2, -0.2)$. The remaining parameters are $b = 0.2$ and $c = 22$.

followed by monostable period-3-oscillations, but the results have not presented here for brevity.

3. Chaos Suppression in SynRM without External Inputs Using Single Controller

In this section, three single controllers are mathematically designed by using the principle of Lyapunov's method for asymptotic global stability to suppress the chaotic behavior found in SynRM without external inputs [29].

3.1. Proposed Controller 1. System (3a)–(3c) with the first single controller $u_1 = -yz$ is described by

$$\frac{dx}{dt} = -bx + yz + u_1, \tag{4a}$$

$$\frac{dy}{dt} = -y - xz + cz, \tag{4b}$$

$$\frac{dz}{dt} = xy - az. \tag{4c}$$

The controlled system (4a)–(4c) can be rewritten as

$$\frac{dx}{dt} = -bx, \tag{5a}$$

$$\frac{dy}{dt} = -y - xz + cz, \tag{5b}$$

$$\frac{dz}{dt} = xy - az. \tag{5c}$$

The solution of equation (5a) is $x(t) = x(0)e^{-bt}$. That is, yield $\lim_{t\longrightarrow\infty} x(t) = 0$. So, system (5a)–(5c) can be reduced as follows:

$$\frac{dy}{dt} = -y + cz, \tag{6a}$$

$$\frac{dz}{dt} = -az. \tag{6b}$$

The solution of equation (6b) is $z(t) = z(0)e^{-at}$. That is, yield $\lim_{t\longrightarrow\infty} z(t) = 0$. So, system (6a) and (6b) can be rewritten as follows

$$\frac{dy}{dt} = -y. \tag{7}$$

The solution of equation (7) is $y(t) = y(0)e^{-t}$. That is, yield $\lim_{t\longrightarrow\infty} y(t) = 0$. Therefore, the chaotic behavior found in the SynRM without external inputs can be controlled using the controller $u_1 = -yz$. The curves of the state responses and the output of the controller 1 are shown in Figure 4.

The results of Figure 4 show the efficiency of the controller u_1.

3.2. Proposed Controller 2. System (3a)–(3c) with the second single controller $u_2 = z(x - c)$ is described by

$$\frac{dx}{dt} = -bx + yz, \tag{8a}$$

$$\frac{dy}{dt} = -y - xz + cz + u_2, \tag{8b}$$

$$\frac{dz}{dt} = xy - az. \tag{8c}$$

The controller u_2 into the controlled system (8a)–(8c) can be rewritten as

$$\frac{dx}{dt} = -bx + yz, \tag{9a}$$

$$\frac{dy}{dt} = -y, \tag{9b}$$

$$\frac{dz}{dt} = xy - az. \tag{9c}$$

The solution of equation (9b) is $y(t) = y(0)e^{-t}$. That is, yield $\lim_{t\longrightarrow\infty} y(t) = 0$. Thus, the system (9a)–(9c) can be reduced as follows:

$$\frac{dx}{dt} = -bx, \tag{10a}$$

$$\frac{dz}{dt} = -az. \tag{10b}$$

The solution of system (10a) and (10b) is given by

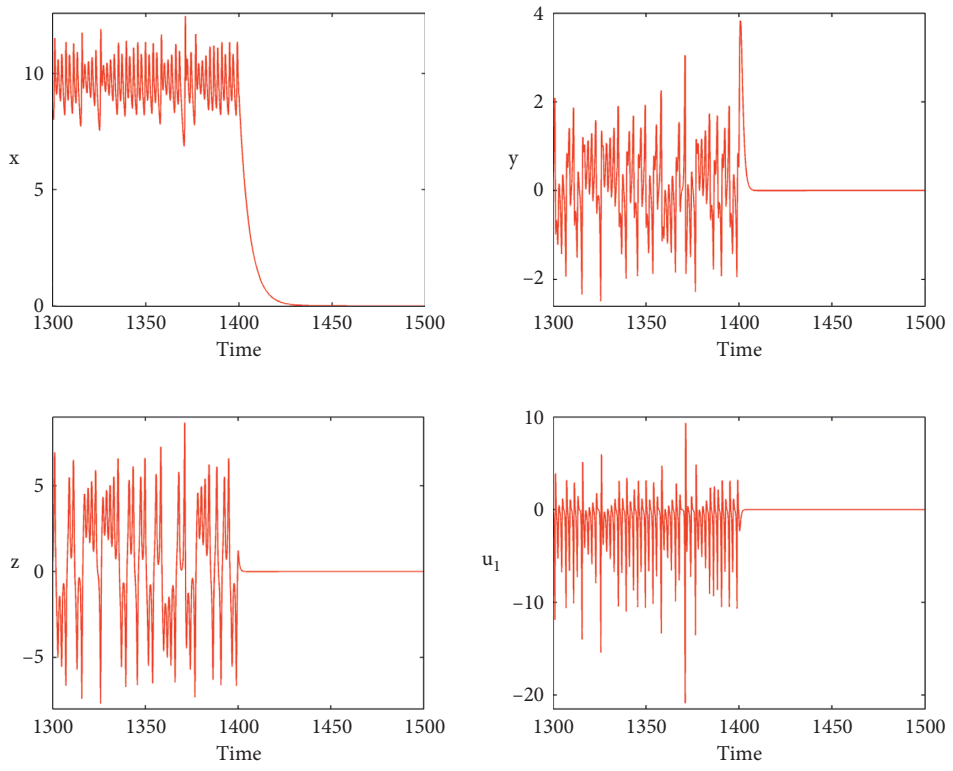

Figure 4: Time series of $x, y, z,\ u_1$ for $a = 3$, $b = 0.2$, and $c = 22$. The initial conditions are (x(0), y(0), z(0)) = (0.1, 0.2, 0.2).

$$x(t) = x(0)e^{-bt}, \tag{11a}$$

$$z(t) = z(0)e^{-at}. \tag{11b}$$

That is, yield $\lim_{t\longrightarrow\infty} y(t) = 0$ and $\lim_{t\longrightarrow\infty} z(t) = 0$. Therefore, the chaotic behavior found in the SynRM without external inputs can be controlled using the controller $u_2 = z(x - c)$. The curves of the state responses and the output of the controller are shown in Figure 5.

The results of Figure 4 reveal the efficiency of the controller u_2.

3.3. Proposed Controller 3. System (3a)–(3c) with the third single controller $u_3 = -xy$ is described by

$$\frac{dx}{dt} = -bx + yz, \tag{12a}$$

$$\frac{dy}{dt} = -y - xz + cz, \tag{12b}$$

$$\frac{dz}{dt} = xy - az + u_3. \tag{12c}$$

Substituting the expression of the controller u_3 into the controlled system (12a)–(12c) becomes

$$\frac{dx}{dt} = -bx + yz, \tag{13a}$$

$$\frac{dy}{dt} = -y - xz + cz, \tag{13b}$$

$$\frac{dz}{dt} = -az. \tag{13c}$$

The solution of equation (13c) is $z(t) = z(0)e^{-at}$. That, is yield $\lim_{t\longrightarrow\infty} z(t) = 0$. Thus, system (13a)–(13c) can be reduced as follows:

$$\frac{dx}{dt} = -bx, \tag{14a}$$

$$\frac{dy}{dt} = -y. \tag{14b}$$

The solution of system (14a) and (14b) can be rewritten as follows:

$$x(t) = x(0)e^{-bt}, \tag{15a}$$

$$y(t) = y(0)e^{-t}. \tag{15b}$$

That is, yield $\lim_{t\longrightarrow\infty} x(t) = 0$ and $\lim_{t\longrightarrow\infty} y(t) = 0$. Therefore, the chaotic behavior found in SynRM without external inputs can be controlled using the controller $u_3 = -xy$. The curves of the state responses and the output of the single controller 3 are shown in Figure 6.

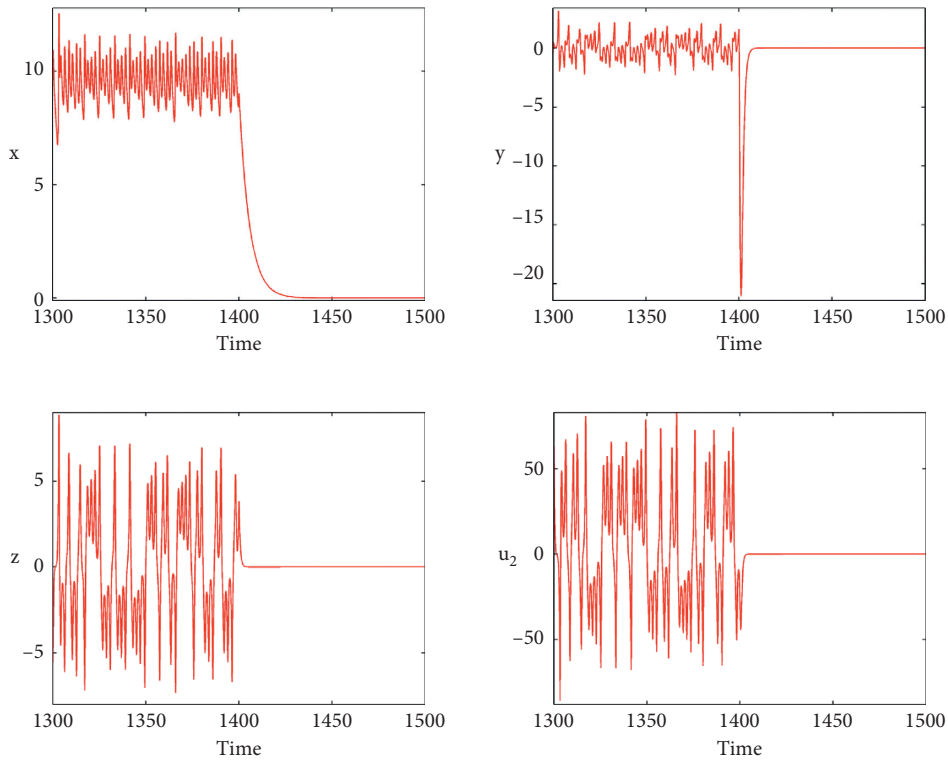

Figure 5: Time series of x, y, z, u_2 for $a = 3$, $b = 0.2$ and $c = 22$. The initial conditions are (x(0), y(0), z(0)) = (0.1, 0.2, 0.2).

The results of Figure 6 show the efficiency of the controller u_3. From practical realization point of view, the single controllers 1 and 3 are preferred because of the inclusion of two states variables (i.e. y and z or x and z) in a single expression signifying a lesser requirement of sensing devices during their fabrication. Hence, this making the system to become cheap.

4. Circuit Implementation of SynRM without External Inputs and Chaos Suppression in SynRM without External Inputs

The electronic implementation of system (3a)–(3c) is depicted in Figure 7.

The electronic circuit of Figure 7 is made of three capacitors, thirteen resistors, six TL081 operational amplifiers, and three analog devices AD633 multipliers. Based on the circuit diagram of Figure 7, the phase portraits of dynamical behaviors found in SynRM without external inputs are illustrated in Figure 8 for specific values of capacitors and resistors.

The good qualitative agreement between the Pspice results of Figure 8 and the numerical simulations results of Figure 3 confirms the existence of the dynamical behavior found in SynRM without external inputs. The electronic implementations of the controlled systems (5a)–(5c), (9a)–(9c), and (13a)–(13c) are deduced from the electronic implementation of system (5a)–(5c) in Figure 7 (not shown). The time series of the state responses and the output of the single controller 1 generated from the circuit diagram of the controlled system (5a)–(5c) are shown in Figure 9.

The good qualitative agreement between the Pspice results of Figure 9 and the numerical simulations results of Figure 5 confirms the efficiency of proposed single controller 3. The time series of the state responses and the output of the single controller 2 generated from the circuit diagram of the controlled system (9a)–(9c) are shown in Figure 10.

The good qualitative agreement between the Pspice results of Figure 10 and the numerical simulations results of Figure 5 confirms the efficiency of proposed single controller 2. The time series of the state responses and the

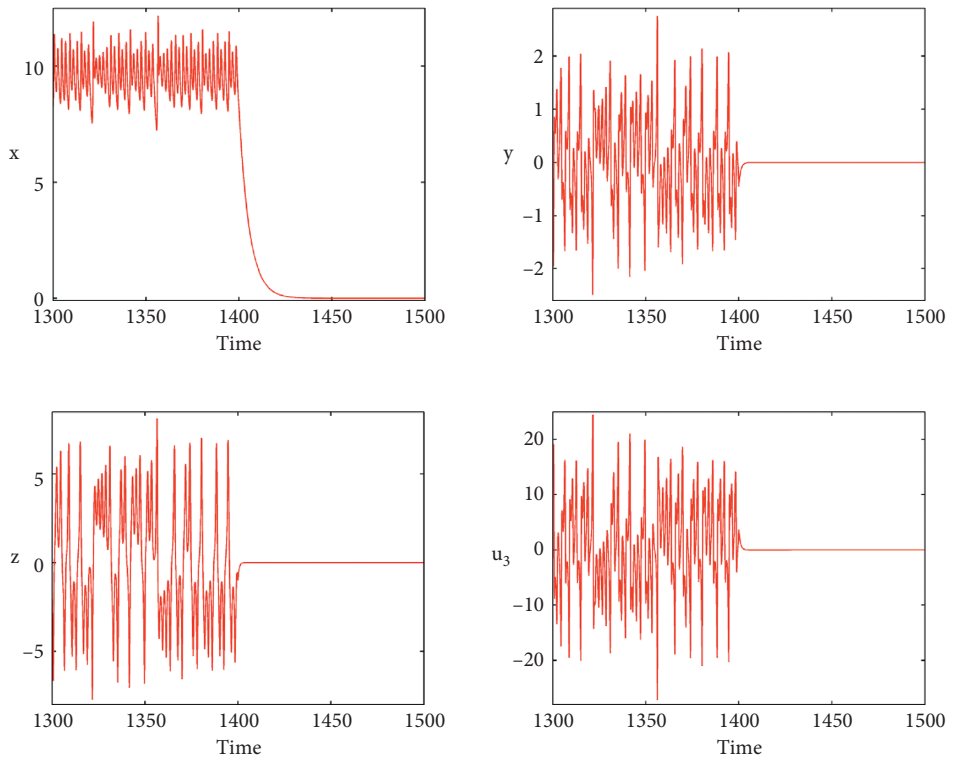

Figure 6: Time series of x, y, z, u_3 for $a = 3$, $b = 0.2$ and $c = 22$. The initial conditions are (x(0), y(0), z(0)) = (0.1, 0.2, 0.2).

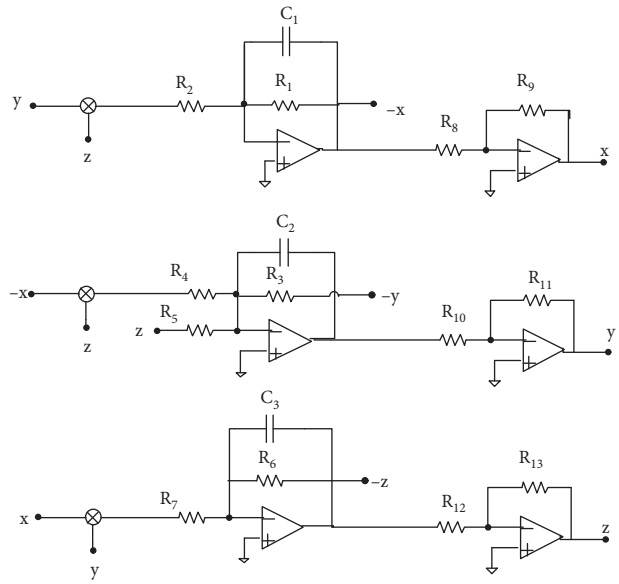

Figure 7: Circuit diagram of system (3a)–(3c) describing SynRM without external inputs.

output of the single controller 3 generated from the circuit diagram of the controlled system (13a)–(13c) are shown in Figure 11.

The good qualitative agreement between the Pspice results of Figure 11 and the numerical simulations results of Figure 6 confirms the efficiency of proposed single controller 3.

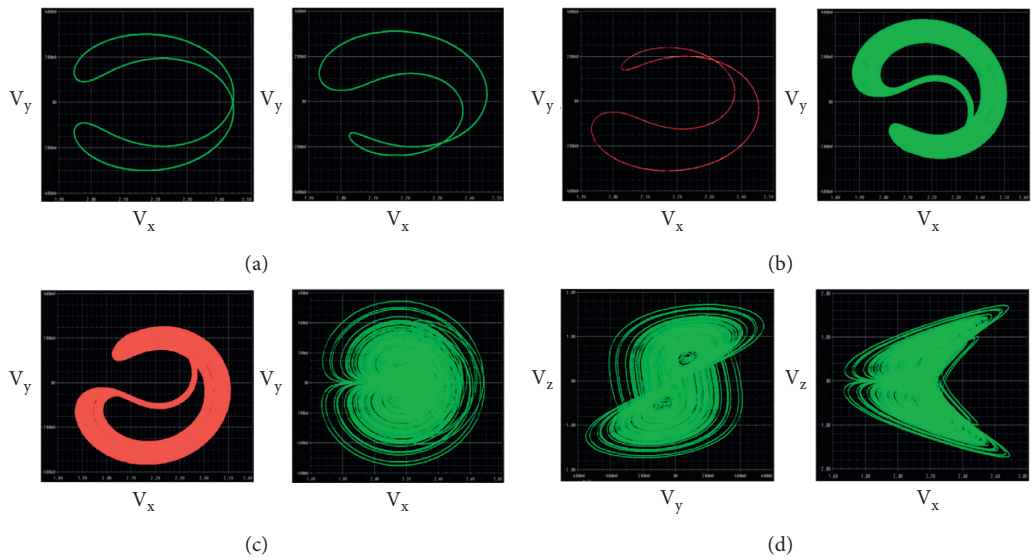

FIGURE 8: Phase planes of the dynamical behaviors of circuit in Figure 7 observed on the Pspice oscilloscope for specific values of R_6: (a) $R_6 = 6.67\,k\Omega$, (b) $R_6 = 5.56\,k\Omega$, (c)$R_6 = 5\,k\Omega$, and (d) $R_6 = 3.33\,k\Omega$. The others values are $C_1 = C_2 = C_3 = 10\,\text{nF}$, $R_3 = R_8 = R_9 = R_{10} = R_{11} = R_{12} = R_{13} = 10\,k\Omega$, $R_5 = 454.55\,k\Omega$, $R_1 = 50\,k\Omega$, $R_2 = R_4 = R_7 = 1\,k\Omega$.

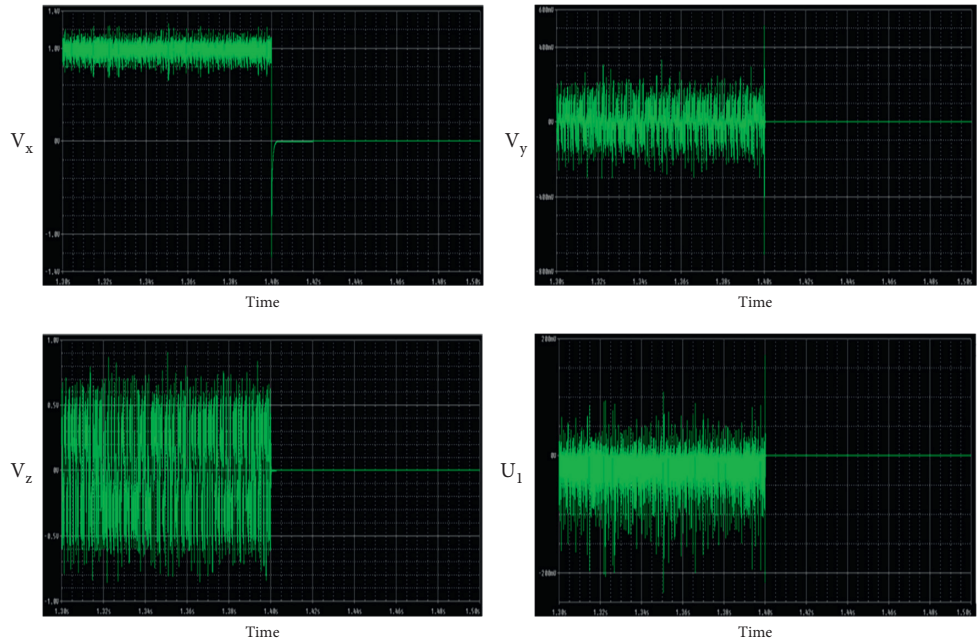

FIGURE 9: Time series of chaos suppression in SynRM without external inputs generated from the Pspice oscilloscope for the capacitors and resistors: $C_1 = C_2 = C_3 = 10\,\text{nF}$, $R_3 = R_8 = R_9 = R_{10} = R_{11} = R_{12} = R_{13} = 10\,k\Omega$, $R_5 = 454.55\,k\Omega$, $R_1 = 50\,k\Omega$, $R_2 = R_4 = R_7 = 1\,k\Omega$, $R_6 = 3.33\,k\Omega$.

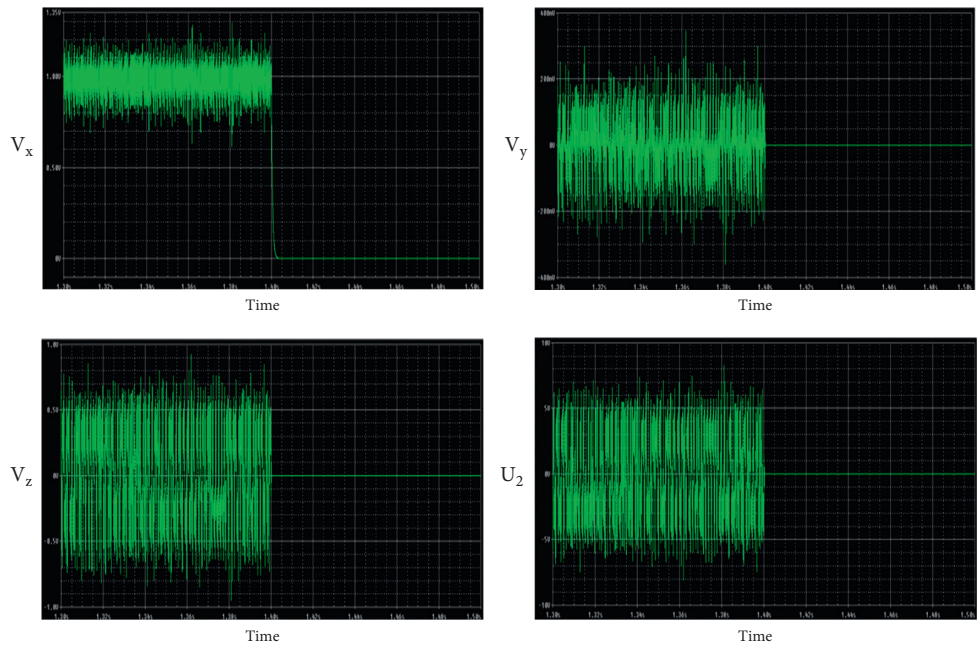

FIGURE 10: Time series of chaos suppression in SynRM without external inputs generated from the Pspice oscilloscope for the capacitors and resistors: $C_1 = C_2 = C_3 = 10\,\text{nF}$, $R_3 = R_8 = R_9 = R_{10} = R_{11} = R_{12} = R_{13} = 10\,k\Omega$, $R_5 = 454.55\,k\Omega$, $R_1 = 50\,k\Omega$, $R_2 = R_4 = R_7 = 1\,k\Omega$, $R_6 = 3.33\,k\Omega$.

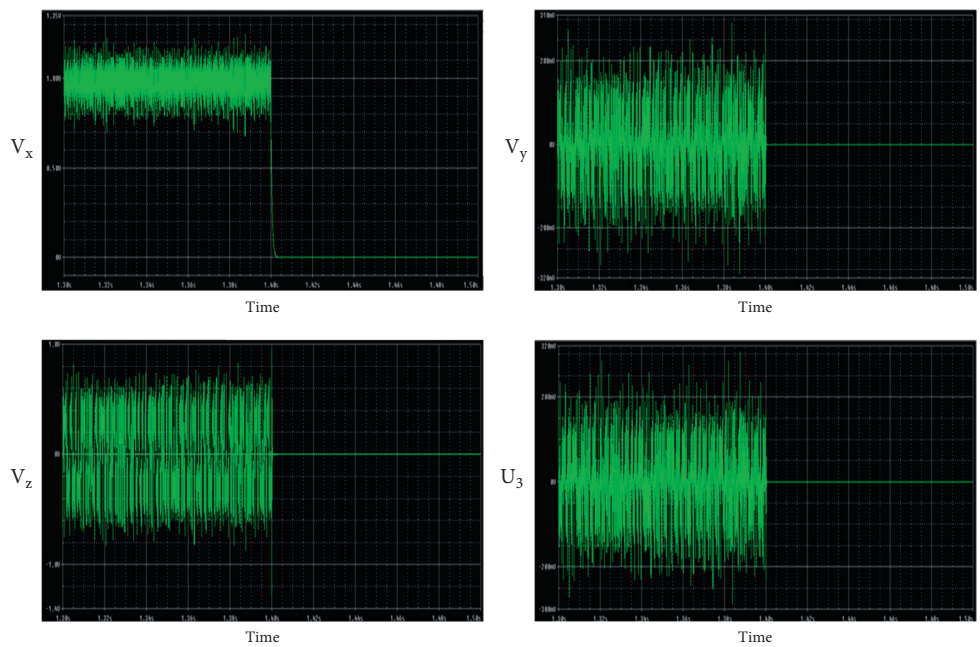

FIGURE 11: Time series of chaos suppression in SynRM without external inputs generated from the Pspice oscilloscope for the capacitors and resistors: $C_1 = C_2 = C_3 = 10\,\text{nF}$, $R_3 = R_8 = R_9 = R_{10} = R_{11} = R_{12} = R_{13} = 10\,k\Omega$, $R_5 = 454.55\,k\Omega$, $R_1 = 50\,k\Omega$, $R_2 = R_4 = R_7 = 1\,k\Omega$, $R_6 = 3.33\,k\Omega$.

5. Conclusion

This paper is dealt with the dynamical analysis, chaos suppression, and electronic implementation of synchronous reluctance motor without external inputs. The numerical analysis of synchronous reluctance motor without external inputs was revealed as monostable periodic attractors, bistable periodic attractors, monostable double-scroll chaotic attractors, and bistable one-scroll chaotic attractors. Thanks to the principle of Lyapunov's method for asymptotic global stability, three single controllers were designed to suppress chaotic behavior found in synchronous

reluctance motor without external inputs, and it was revealed that they were simple and easy to implement. The single controllers 1 and 3 could be a preferable choice because of the use of two states variables (i.e. y and z or x and z) in a single expression. Numerical simulations results were provided to demonstrate the efficiency of three proposed single controllers. To access the physical feasibility of three designed single controllers and the existence of the dynamical behaviors found in synchronous reluctance motor without external inputs, electronic circuits were implemented and validated on OrCAD-PSpice software. In the future works, it will be interesting to study the synchronous reluctance motor with external inputs such as the load torque and the stator voltage.

Data Availability

The data used to support the findings of this study are included within the article.

Conflicts of Interest

The authors declare that they have no conflicts of interest.

Acknowledgments

This work was partially funded by the Center for Nonlinear Systems, Chennai Institute of Technology, India via funding number CIT/CNS/2021/RD/064.

References

[1] A. E. Fitzgerald, C. Jr. Kingsley, and S. D. Umpans, *Electric Machinery*, McGraw-Hill, New York, NY, USA, 1991.

[2] J. Machowski, J. Bialek, and J. R. Bumby, *Power System Dynamics and Stability*, John Wiley & Sons, Hoboken, NJ, USA, 1997.

[3] A. Parra, A. Zubizarreta, J. Pérez, and M. Dendaluce, "Intelligent torque vectoring approach for electric vehicles with per-wheel motors," *Complexity*, vol. 2018, Article ID 7030184, 14 pages, 2018.

[4] F. Stîngă, M. Marian, and D. Selisteanu, "Robust estimation-based control strategies for induction motors," *Complexity*, vol. 2020, Article ID 9235701, 14 pages, 2020.

[5] Q. Ji and M. Ye, "Control of chaotic calcium oscillations in biological cells," *Complexity*, vol. 2021, Article ID 8861465, 14 pages, 2021.

[6] X. Hu and P. Zhou, "Coexisting three-scroll and four-scroll chaotic attractors in a fractional-order system by a three-scroll integer-order memristive chaotic system and chaos control," *Complexity*, vol. 2020, Article ID 5796529, 7 pages, 2020.

[7] I. Nagy, Z. Siitb, and L. Backhausz, "Periodic states of hysteresis current control of I.M," in *Proceedings of the 29th International Power Conversion and Intelligent Motion Conference (PCIM'SG)*, pp. 605–619, Nürnberg, Germany, May 1996.

[8] Z. Suto, I. Nagy, and Z. Jak, "Periodic responses of a nonlinear current conti-olled IM drive," in *Proceedings of the 7th European Conference on Power Electronics and Applications (EPE'S'I)*, vol. 3, Trondheim, Norway, September 1997.

[9] Z. Zhong Li, J. B. Jin Bae Park, Y. H. Young Hoon Joo, B. Bo Zhang, and G. Guanrong Chen, "Bifurcations and chaos in a permanent-magnet synchronous motor," *IEEE Transactions on Circuits and Systems I: Fundamental Theory and Applications*, vol. 49, no. 3, pp. 383–387, 2002.

[10] P. Pillay and R. Krishnan, "Modeling, analysis and simulation of a high performance vector controlled, permanent magnet synchronous motor drive," *Rec. Conf. IEEE-IAS Annul. Meeting*, pp. 253–262, 1987.

[11] N. Hemati, "Dynamic analysis of brushless motors based on compact representations of motion," in *Proceedings of the Conference Record of the IEEE Industry Applications Society Annual Meeting*, vol. 1, pp. 51–58, Toronto, ON, Canada, October 1993.

[12] N. Hemati, "Strange attractors in brushless DC motors," *IEEE Transactions on Circuits and Systems I: Fundamental Theory and Applications*, vol. 41, no. 1, pp. 40–45, 1994.

[13] Y. Gao and K. T. Chau, "Hopf bifurcation and chaos in synchronous reluctance motor drives," *IEEE Transactions on Energy Conversion*, vol. 19, no. 2, pp. 296–302, 2004.

[14] P. J. Lawrenson, "A brief status review of switched reluctance drives," *EPE Journal*, vol. 2, no. 3, pp. 133–144, 1992.

[15] C. C. Chan, Y. Zhan, Q. Jiang, and K. T. Chau, "A high performance switched reluctance motor drive for P-star EV project," in *Proceedings of the 13th International Electric Vehicle Symposium*, pp. 78–83, Osaka Japan, October 1996.

[16] N. Bianchi, S. Bolognani, D. Bon, and M. Dai Pre, "Torque harmonic compensation in a synchronous reluctance motor," *IEEE Transactions on Energy Conversion*, vol. 23, no. 2, pp. 466–473, 2008.

[17] M. Ferrari, N. Bianchi, A. Doria, and E. Fornasiero, "Design of synchronous reluctance motor for hybrid electric vehicles," *IEEE Transactions on Industry Applications*, vol. 51, no. 4, pp. 3030–3040, 2015.

[18] J. Kolehmainen, "Synchronous reluctance motor with form blocked rotor," *IEEE Transactions on Energy Conversion*, vol. 25, no. 2, pp. 450–456, 2010.

[19] S. T. Kingni, A. Cheukem, P. R. N. Tuwa, A. C. Chamgoué, V.-T. Pham, and S. Jafari, "Synchronous reluctance motor with load vibration perturbation: analysis, electronic implementation and adaptive backstepping sliding mode control," *Iranian Journal of Science and Technology, Transactions of Electrical Engineering*, vol. 45, no. 2, pp. 645–654, 2021.

[20] K. T. Chau and Z. Wang, *Chaos in Electric Drive Systems: Analysis, Control and Application*, John Wiley & Sons, Hoboken, NJ, USA, 2011.

[21] W. Du-Qu and L. Xiao-Shu, "Passive adaptive control of chaos in synchronous reluctance motor," *Chinese Physics B*, vol. 17, no. 1, pp. 92–97, 2008.

[22] M. Babaei, J. Nazarzadeh, and J. Faiz, "Nonlinear feedback control of chaos in synchronous reluctance motor drive systems," in *Proceedings of the IEEE conference Industrial Technology*, pp. 1–5, Chengdu, China, April 2008.

[23] F. Q. Tang, Y. N. Tong, and C. L. Li, "A controller for chaotic synchronous reluctance motor drive systems," in *Proceedings of the IEEE conference Computing, Control and Industrial Engineering*, pp. 316–319, Wuhan, China, September 2011.

[24] L. Xu, X. Xu, T. A. Lipo, and D. W. Novotny, "Vector control of a synchronous reluctance motor including saturation and Iron Loss," *IEEE Transactions on Industry Applications*, vol. 27, no. 5, pp. 977–985, 1991.

[25] M. K. Metwally and M. E. Ahmed, "Vector control of four switch three-phase inverter fed synchronous reluctance motor drive including saturation and iron losses effects based Maximum Torque Control," *Telkomnika*, vol. 11, pp. 6344–6351, 2013.

[26] E. M. Rashad, T. S. Radwan, and M. A. Rahman, "A maximum torque per ampere vector control strategy for synchronous reluctance motors considering saturation and iron losses, 39th IAS Annual Meeting," in *Proceedings of the IEEE Industry Applications Conference*, vol. 4, pp. 2411–2417, Seattle, WA, USA, October 2004.

[27] M. A. Fellani and D. E. Abaid, "Sliding-mode control of synchronous reluctance motor," *International Journal of Electronics, Circuits and Systems*, vol. 3, pp. 91–95, 2009.

[28] K. Rajagopal, F. Nazarimehr, A. Karthikeyan, A. Srinivasan, and S. Jafari, "Fractional order synchronous reluctance motor: analysis, chaos control and fpga implementation," *Asian Journal of Control*, vol. 20, pp. 1–15, 2018.

[29] X. Liao and P. Yu, *Absolute Stability of Nonlinear Control Systems*, Springer Science & Business Media, Berlin, Germany, 2008.